

Numerical study on self-sustainable atmospheric boundary layer considering wind veering based on steady k - ε model

Chengdong Feng^a and Ming Gu*

State Key Laboratory for Disaster Reduction in Civil Engineering, Tongji University, Shanghai, 200092, China

(Received April 3, 2019, Revised July 9, 2019, Accepted August 7, 2019)

Abstract. Modelling incompressible, neutrally stratified, barotropic, horizontally homogeneous and steady-state atmospheric boundary layer (ABL) is an important aspect in computational wind engineering (CWE) applications. The ABL flow can be viewed as a balance of the horizontal pressure gradient force, the Coriolis force and the turbulent stress divergence. While much research has focused on the increase of the wind velocity with height, the Ekman layer effects, entailing veering — the change of the wind velocity direction with height, are far less concerned in wind engineering. In this paper, a modified k - ε model is introduced for the ABL simulation considering wind veering. The self-sustainable method is discussed in detail including the precursor simulation, main simulation and near-ground physical quantities adjustment. Comparisons are presented among the simulation results, field measurement values and the wind profiles used in the conventional wind tunnel test. The studies show that the modified k - ε model simulation results are consistent with field measurement values. The self-sustainable method is effective to maintain the ABL physical quantities in an empty domain. The wind profiles used in the conventional wind tunnel test have deficiencies in the prediction of upper-level winds. The studies in this paper support future practical super high-rise buildings design in CWE.

Keywords: computational wind engineering; atmospheric boundary layer; self-sustainable method; modified k - ε model; Coriolis force

1. Introduction

Being able to model incompressible, neutrally stratified, barotropic, horizontally homogeneous and steady-state atmospheric boundary layer (ABL) in computational fluid dynamics (CFD) is an important precondition for modelling flow around buildings (Yang *et al.* 2008, Yang *et al.* 2009, Zheng *et al.* 2012, Yang *et al.* 2017). The ABL, with a height that typically varies from 1-1.5 km (Tse *et al.* 2016), consists of the atmospheric surface layer (ASL) and the Ekman layer, as shown in Fig. 1. Generally, the ABL flow can be approximately viewed as a balance of the horizontal pressure gradient force, the Coriolis force and the turbulent stress divergence. While much research has focused on the increase of the wind velocity with height, the Ekman layer effects, entailing veering -- the change of the wind velocity direction with height, are far less concerned in wind engineering.

Recently, there have been many super high-rise buildings over 500 m worldwide, such as the Shanghai Tower (632 m), Burj Khalifa Tower (828 m), etc. For these super high-rise buildings, high-altitude wind characteristics will have a great impact on wind loads and wind-induced responses, and may even be decisive. The wind veering will obviously make the bottom and top sections of the structure under different excitations, and may cause complex coupled vibrations, which should be given enough attention in the

design of thousand-meter super high-rise buildings. However, there has been very little research on the influence of wind veering on high-rise buildings so far, due to the difficulty of simulating veering in conventional boundary layer wind tunnels. Yeo (2012) developed a practical procedure within a database-assisted design framework that approximately accounted for veering effects on the Commonwealth Advisory Aeronautical Research Council (CAARC) standard building model, and the veering effects were found to be small. However, the building chosen in the study had a height of only 182.88 m, and the veering effects were assumed to be uniform over the entire building height rather than gradually varying from the ground to the top of the building. Some studies have focused on simulating twisted wind profiles to investigate wind veering effects. Tse *et al.* (2016) proposed to employ twisted wind profiles in wind tunnel tests involving installed vane systems to research the urban pedestrian level wind (PLW) field of Hong Kong. Weerasuriya *et al.* (2018) proposed a new set of inflow boundary conditions to model twisted wind flows in CFD simulations. However, the twisted wind profiles in these studies were formed by topography instead of the Coriolis force and were confined to the lower 500 m of the ABL. Additionally, the simulated twisted wind profiles in wind tunnel tests and CFD followed the power law and the logarithmic law, respectively, which are not appropriate for describing the entire ABL (Li *et al.* 2017).

For reliable studies on the structural wind engineering of super high-rise buildings, the precise simulation of wind flow needs to be achieved. In the present study, a modified

*Corresponding author, Professor,

E-mail: minggu@tongji.edu.cn

^a Ph.D. Student, E-mail: 1510177@tongji.edu.cn

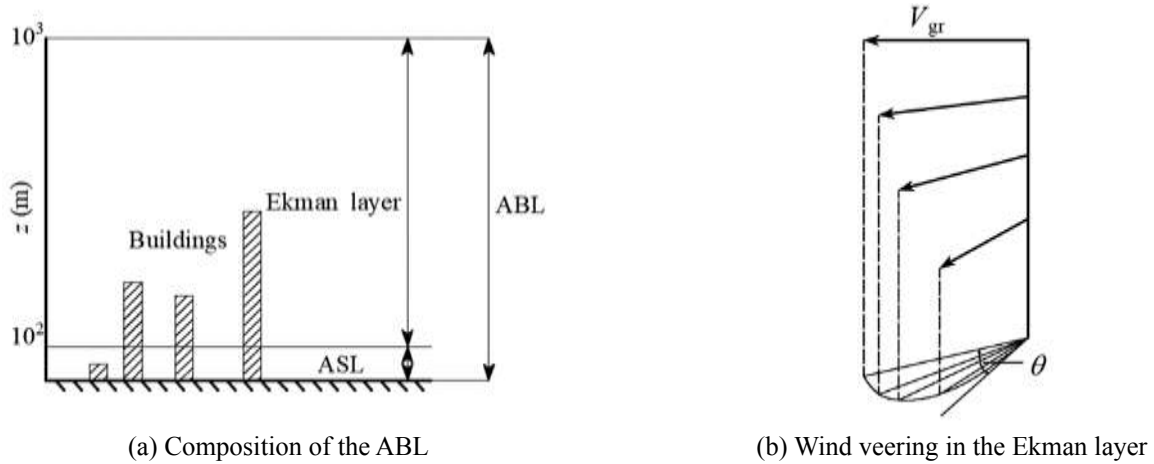


Fig. 1 Composition of the ABL and wind veering in the Ekman layer (Simiu and Scanlan 1996)

k - ϵ model is introduced for the ABL simulation considering wind veering. The self-sustainable method is discussed in detail including the precursor simulation, main simulation and near-ground physical quantities adjustment. The computational results are compared with field measurement data to verify the accuracy and effectiveness of the proposed method. Besides, the deficiencies of the wind profiles used in the conventional wind tunnel test are provided. The research of this paper is expected to be referred to for the wind-resistance design of thousand-meter super high-rise buildings.

2. Methodology and results

In this section, we attempt to propose an approach to simulate the self-sustainable ABL considering wind veering with height accurately. First, the development of consistent inflow profiles in the precursor simulation using a modified k - ϵ model is explained in Subsection 2.1. The profiles are then applied as inflow conditions for empty domains in the main simulation to determine whether the flow maintains its homogeneity in Subsection 2.2. Finally, Subsection 2.3 provides the method of near-ground physical quantities adjustment to achieve better self-sustaining results.

2.1 Precursor simulation

The precursor simulation generates a library of turbulence databases that possess required flow characteristics such as mean velocity, turbulent kinetic energy and turbulent dissipation rate. Once the desired turbulence flow characteristics are achieved, the field data will be extracted and stored. Since the ABL studied in this paper is horizontally homogeneous and at the steady state, a small number of grid elements can be used in the precursor simulation for calculating inflow profiles that are consistent with the turbulence model and ground boundary condition. This approach is sometimes used in meteorology models (Franke *et al.* 2007), and it has also been suggested by Blocken *et al.* (2007). The advantage of this approach is that the profiles are guaranteed to be consistent with the

ground boundary condition. It has the additional benefit that it can be applied regardless of the wall function model used at the ground and also regardless of the turbulence model used (O'Sullivan *et al.* 2011). It should be mentioned that if the artificially designated wind profiles are directly applied as inflow conditions for empty domains in the subsequent main simulation rather than calculated from the precursor simulation, the self-sustaining wind field will not necessarily be achieved well.

2.1.1 Modified k - ϵ model

Under neutral stratification, the horizontal momentum equations for a horizontally homogeneous and steady-state ABL can be written in Cartesian coordinates as

$$-\frac{1}{\rho} \frac{\partial p}{\partial x} + fv - \frac{\partial \overline{u'w'}}{\partial z} = 0 \quad (1)$$

$$-\frac{1}{\rho} \frac{\partial p}{\partial y} - fu - \frac{\partial \overline{v'w'}}{\partial z} = 0 \quad (2)$$

where (u, v) are components of mean velocity; p and ρ denote the air pressure and the air density respectively; f is the Coriolis parameter ($f = 2\omega \sin \varphi$, where φ is the latitude, and ω is the angular velocity of the Earth rotation); $-\overline{u'w'}$ and $-\overline{v'w'}$ are (kinetic) turbulent stress components. These equations express a balance of three forces: the horizontal pressure gradient force, the Coriolis force and the turbulent stress divergence (Cai *et al.* 2014), and are also called the classical Ekman model.

The Reynolds-averaged approach to turbulence modelling requires that the turbulent stress components are appropriately modelled. A common method employs the Boussinesq hypothesis to relate the Reynolds stresses to the mean velocity gradients

$$-\overline{\rho u_i u_j} = \mu_t \left(\frac{\partial u_i}{\partial x_j} + \frac{\partial u_j}{\partial x_i} \right) - \frac{2}{3} \rho k \delta_{ij} \quad (3)$$

where u_i represent the velocities in three orthogonal directions; x_i denote three orthogonal directions; μ_t is the

turbulent viscosity; k is the turbulent kinetic energy; and δ_{ij} is the Kronecker symbol.

Introducing the assumption that the ABL is incompressible, neutrally stratified, barotropic, horizontally homogeneous and steady-state, and ignoring the molecular viscosity, the standard k - ε model can be expressed as follows (Launder and Spalding 1974)

$$\frac{\partial}{\partial x_j} \left(\frac{\mu_t}{\sigma_k} \frac{\partial k}{\partial x_j} \right) + G_k - \rho \varepsilon + S_k = 0 \quad (4)$$

$$\frac{\partial}{\partial x_j} \left(\frac{\mu_t}{\sigma_\varepsilon} \frac{\partial \varepsilon}{\partial x_j} \right) + C_{1\varepsilon} \frac{\varepsilon}{k} G_k - C_{2\varepsilon} \rho \frac{\varepsilon^2}{k} + S_\varepsilon = 0 \quad (5)$$

$$\mu_t = \rho C_\mu \frac{k^2}{\varepsilon} \quad (6)$$

where G_k represents the generation of turbulence kinetic energy due to the mean velocity gradients; k and ε are the turbulent kinetic energy and its dissipation rate; S_k and S_ε are user-defined source terms; $C_{1\varepsilon}$, $C_{2\varepsilon}$ and C_μ are constants; σ_k and σ_ε are the turbulent Prandtl numbers for k and ε , respectively.

However, many meteorological researchers (Detering and Etling 1985, Duynkerke 1988, Apsley and Castro 1997, Sogachev *et al.* 2012) found that when the standard k - ε model was directly used to simulate the ABL, compared with the field measurement data (Lettau 1950), the mean wind velocity magnitude and mean wind veering were significantly underestimated, and there was no obvious inflection point in the mean wind profile. In order to solve this problem, they proposed their own approaches, of which the method proposed by Apsley and Castro (1997) was relatively effective. The main idea is to modify the transport equation of ε and replace $C_{1\varepsilon}$ in the ε equation with $C_{1\varepsilon}^*$ as follows

$$C_{1\varepsilon}^* = C_{1\varepsilon} + (C_{2\varepsilon} - C_{1\varepsilon}) \frac{l_m}{l_{\max}} \quad (7)$$

$$l_m = \frac{C_\mu^{3/4} k^{3/2}}{\varepsilon} \quad (8)$$

where l_{\max} represents the maximum mixing length of the ABL, and l_m is the local mixing length (i.e., the turbulence length scale). When $l_m \ll l_{\max}$ (i.e., close to the surface) the change is negligible and the equations remain consistent with the standard k - ε model. On the other hand, assuming local equilibrium ($G_k = \rho \varepsilon$), then source and sink terms in the ε equation will cancel when $l_m = l_{\max}$. The Eq. (7) therefore acts as a feedback mechanism to oppose the turbulent length scale exceeding l_{\max} , and with the exception of l_{\max} , the modification introduces no new constants into the model and may be applied with any a priori values of $C_{1\varepsilon}$ and $C_{2\varepsilon}$. The steady k - ε model with the Eq. (7) is referred to as “modified k - ε model” hereinafter.

2.1.2 Simulations and implementations

In order to computationally verify the capability of the modified k - ε model to simulate the ABL, numerical

simulations in domains without obstacles are carried out by utilizing the commercial software ANSYS Fluent 15.0. The implementation procedure for the precursor simulation is as follows.

Target wind profile

The famous “Leipzig Wind Profile” is specified as the target wind profile for the ABL numerical simulation. The “Leipzig Wind Profile” is a typical example of a representative wind distribution in the ABL which resulted from MILDNER’s set of 28 pilot-balloon observations with two theodolites on October 20, 1931, near Leipzig for a nominally neutral weather situation (Lettau 1950). The wind parameters of the “Leipzig Wind Profile” are shown in Table 1, where G is the geostrophic wind velocity magnitude, φ is the latitude, u^* is the friction velocity, z_0 is the aerodynamic roughness length, f is the Coriolis parameter, and θ_0 is the angle between the horizontal wind velocity vector at the ground level ($z = 0$) and the horizontal geostrophic wind velocity vector ($z \approx 1000$ m). In the present study, the direction parallel to the geostrophic wind velocity vector is specified as the x -axis, and the direction perpendicular to the geostrophic wind velocity vector is the y -axis, leading to the components of geostrophic wind velocity $(u_g, v_g) = (G, 0)$.

It is worth mentioning that the Leipzig data set has played a significant role in the development of computational models of ABL flows, even though it is relatively old (Riopelle and Stubble 1989). In the past decades, numerous field measurements and numerical simulation studies have been widely conducted, based on the modern measurement techniques (Tamura *et al.* 2001, Tamura *et al.* 2007, He *et al.* 2013, Peña *et al.* 2014, Liu *et al.* 2018) and advanced numerical simulation methods (Andren *et al.* 1994, Zilitinkevich and Esau 2002, Esau 2004, Zilitinkevich *et al.* 2007, Pedersen *et al.* 2014). However, the Leipzig data are still useful, primarily because the observations were made in a region of relatively steady barotropic atmospheric conditions with a mild stable stratification and the wind data are representative of wind profiles that are in equilibrium with a uniform and flat surface (Lettau 1950, Riopelle and Stubble 1989).

To further prove this point, Fig. 2(a) shows the normalized mean wind velocity magnitude of “Leipzig Wind Profile” (Lettau 1950), and some field measurement data from Liu *et al.* (2018) (“ V_3 , θ_2 ” corresponds to the results with reference wind velocity 15-20 m/s and reference wind direction 90°-180° at flat terrain, see Liu *et al.* 2018 for details), numerical simulation results from Esau (2004) (“ $h = 2000$ m” corresponds to the results with the ABL height of 2000 m, see Esau 2004 for details) and Pedersen *et al.* (2014) (“Case n_{02} ” corresponds to the results of a “conventionally neutral” case, see Pedersen *et al.* 2014 for details) are also included for comparisons. It should be noted that the ABL height h , which is used to normalize the vertical coordinate z , is controlled by numerous factors of different natures. In view of the loss of information on the ABL height h in the research of Lettau (1950), the following calculation of h for “conventionally neutral” flows have been taken (Zilitinkevich *et al.* 2007)

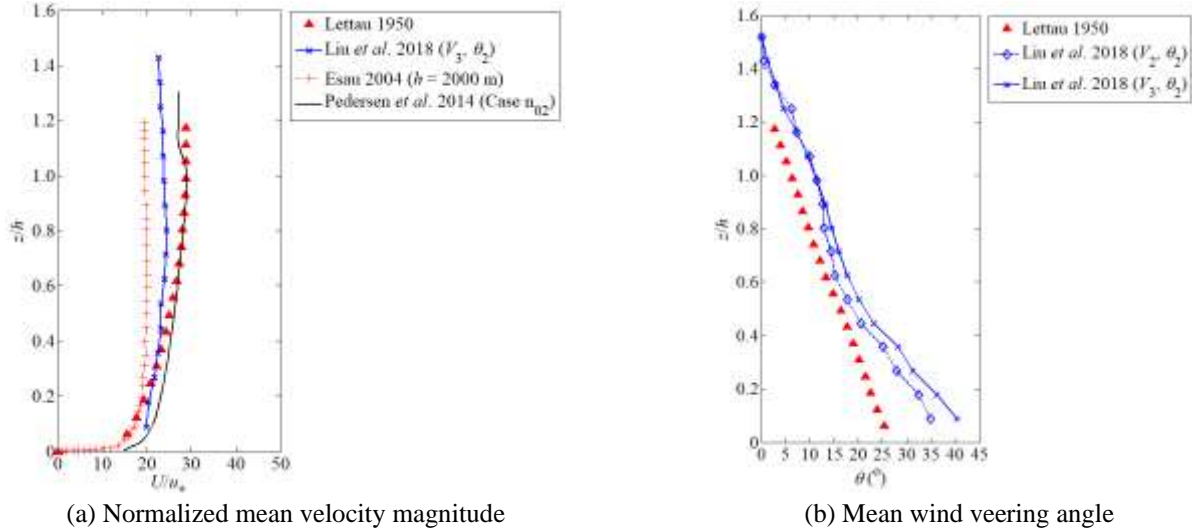


Fig. 2 Comparisons of mean wind profiles between the “Leipzig Wind Profile” and other relevant data

$$\frac{1}{h^2} = \frac{f^2}{(C_R u_*^2)} + \frac{N|f|}{(C_{CN} u_*^2)} \quad (9)$$

where N is the Brunt-Väisälä frequency with a typical value $N = 0.01 \text{ s}^{-1}$ in the free atmosphere, and C_R and C_{CN} are dimensionless empirical constants with recommended values $C_R = 0.6$, $C_{CN} = 1.36$, respectively. The Eq. (9) gives the ABL height $h \approx 808 \text{ m}$ for “Leipzig Wind Profile”. Besides, Fig. 2(b) depicts the comparison results of mean wind veering angle between the “Leipzig Wind Profile” and some field measurement data from Liu *et al.* (2018) (“ V_2, θ_2 ” corresponds to the results with reference wind velocity 10-15 m/s and reference wind direction 90° - 180° at flat terrain, and “ V_3, θ_2 ” corresponds to the results with reference wind velocity 15-20 m/s and reference wind direction 90° - 180° at flat terrain, see Liu *et al.* 2018 for details). It can be observed from Figs. 2(a) and 2(b) that the normalized mean wind velocity magnitude and mean wind veering angle of “Leipzig Wind Profile” could typically reflect the variation tendency of mean wind profiles obtained by advanced measurement techniques and numerical simulations. Therefore, it is reasonable to designate the “Leipzig Wind Profile” as the target wind profile for the ABL numerical simulation herein.

Similarity criteria and scale ratios

The scaled models are usually used in wind tunnel tests and numerical simulations. For the numerical simulations in this paper, the geometric scale ratio $\lambda_L = 1:1333$, the wind velocity scale ratio $\lambda_V = 1:1.12$, and the density scale ratio $\lambda_\rho = 1:1$ are taken as the basic scale ratios to ensure that the scaled values of u_* and z_0 correspond to the experimental data from Zheng *et al.* (2012). Based on these three basic scale ratios, the similarity of Rossby number, i.e., Ro , is considered. The Rossby number Ro in dynamic meteorology is defined as follows

$$Ro = \frac{V}{fL} \quad (10)$$

Table 1 “Leipzig Wind Profile” parameters

Case	$G \text{ (m}\cdot\text{s}^{-1})$	$\varphi \text{ (}^\circ)$	$u_* \text{ (m}\cdot\text{s}^{-1})$	$z_0 \text{ (m)}$	$f \text{ (s}^{-1})$	$\theta_0 \text{ (}^\circ)$
Prototype	17.5	51	0.65	0.30	1.13×10^{-4}	26.1
Scaled model	15.5	51	0.577	2.25×10^{-4}	0.134	26.1

where V denotes the characteristic velocity; L represents the characteristic length; and f is the Coriolis parameter. The scale ratio of the Coriolis parameter λ_f can be derived from the Rossby number similarity criterion

$$\lambda_f = \frac{\lambda_V}{\lambda_L} \approx 1190:1 \quad (11)$$

The scaled wind parameters of the “Leipzig Wind Profile” are also summarized in Table 1.

Mesh discretization

The precursor simulations on different meshes are performed to check the requirement of mesh independence. The details about the three mesh discretization schemes are listed in Table 2. The size of the precursor simulation domain is $L \times B \times H = 1 \text{ m} \times 1 \text{ m} \times 3 \text{ m}$ whose height coincides with the height of the main simulation domain in the with the height of the main simulation domain in the following section. The mesh size in horizontal and lateral direction is uniform and equals to 0.1 m, while the height of the first mesh layer above ground, Δ_m , and the vertical growing factor are set differently for the three meshes. It should be noted that the height of the first mesh layer above ground needs to be set greater than $2K_s$ ($K_s = 9.793z_0/C_s$ is the sand-grain roughness height in the Fluent model, where C_s is the roughness constant that takes a default value of 0.5, see Blocken *et al.* 2007).

Model constants

The values of the turbulence model constants vary with the research issues. Previous measurements showed that the

Table 2 Mesh discretization schemes for precursor simulations

Cases	Number of cells ($N_x \times N_y \times N_z$)*	Height of the first mesh layer above ground Δ_m (m)	Vertical growing factor	Dimensionless wall unit y^+
Mesh-a	$10 \times 10 \times 50$	0.01	1.06	292
Mesh-b	$10 \times 10 \times 50$	0.02	1.04	498
Mesh-c	$10 \times 10 \times 30$	0.04	1.06	923

* N_x : The number of cells along the x direction; N_y : The number of cells along the y direction;
 N_z : The number of cells along the z direction

turbulence level in the ABL near the ground was usually higher than the quantity determined by the relation $k = 3.33u_*^2$ (Richards and Hoxey 1993). The result suggests that C_μ should be less than its default value 0.09, and $C_\mu = 0.03$ is more reasonable (Yang *et al.* 2009, Koblitz *et al.* 2015). According to the research of Koblitz *et al.* (2015), the values of $C_{1\varepsilon}$ and $C_{2\varepsilon}$ are taken as 1.52 and 1.833, respectively. To ensure that the model solution agrees with the constant-stress logarithmic wind profile near the ground, the relation has to be satisfied (Richards and Hoxey 1993)

$$\sigma_\varepsilon = \frac{\kappa^2}{C_\mu^{1/2}(C_{2\varepsilon} - C_{1\varepsilon})} \quad (12)$$

where κ is the von Karman constant with the value of 0.42. According to the research of Poroseva and Iaccarino (2001), the relationship between the coefficients σ_k and σ_ε is more important for the model accuracy than their absolute values, and a constant ratio $\sigma_\varepsilon/\sigma_k = 1.5$ was recommended for practical purposes (Poroseva and Iaccarino 2001).

Additionally, it should be noted that the maximum mixing length of the ABL, l_{\max} , is the new constant in the modified k - ε model. For neutrally stratified ABL flows over a flat rough surface, l_{\max} could be estimated by an expression from Blackadar (1962)

$$l_{\max} = 0.00027 \frac{G}{f} \quad (13)$$

where G is the geostrophic wind velocity magnitude and f is the Coriolis parameter. The Eq. (13) yields a maximum mixing length of the ABL $l_{\max} \approx 41.8$ m for the prototype of "Leipzig Wind Profile", while Apsley and Castro (1997) suggested $l_{\max} = 36$ m for their simulation. It is generally accepted that the Leipzig data were actually recorded in a slightly stable weather situation (Lettau 1950, Riopelle and Stublely 1989). According to the research of Koblitz *et al.* (2015), the measured and simulated profiles agree perfectly when using a lower length scale of $l_{\max} = 28$ m (prototype), which is adopted in this paper. Table 3 shows the standard k - ε model constants (Launder and Spalding 1974) and the modified k - ε model constants.

Boundary conditions and solving settings

The boundary conditions for precursor simulations are shown in Fig. 3. Lateral boundaries are defined as periodic. The top boundary uses a symmetry condition. The bottom wall boundary uses the Scalable Wall Functions with the

Table 3 Model constants

Model constants	C_μ	$C_{1\varepsilon}$	$C_{2\varepsilon}$	σ_k	σ_ε	l_{\max} (m)
Standard k - ε model	0.09	1.44	1.92	1.0	1.3	—
Modified k - ε model	0.03	1.52	1.833	2.169	3.254	28

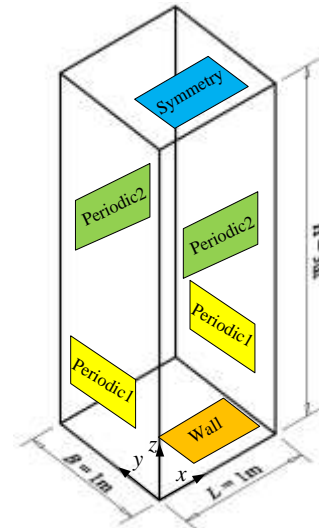


Fig. 3 Boundary conditions for precursor simulations

roughness height $K_s = 0.0044$ m and the roughness constant $C_s = 0.5$.

The flow field is initialized by uniform velocity ($u = 15.5 \text{ m}\cdot\text{s}^{-1}$, $v = 0$, $w = 0$), zero gauge pressure, uniform turbulent kinetic energy ($k = 1 \text{ m}^2\cdot\text{s}^{-2}$), and uniform turbulent dissipation rate ($\varepsilon = 1 \text{ m}^2\cdot\text{s}^{-3}$). In order to drive the flow, the horizontal pressure gradient force needs to be applied. Considering that in a barotropic atmosphere, the horizontal pressure gradient does not change with height, the horizontal pressure gradient force can be deduced from the geostrophic balance between the pressure gradient force and the Coriolis force at the top of the ABL (Cai *et al.* 2014)

$$\frac{\partial p}{\partial x} = \rho f v_g = 0 \quad (14)$$

$$\frac{\partial p}{\partial y} = -\rho f u_g \approx -2.5443 \text{ N}\cdot\text{m}^{-3} \quad (15)$$

where (u_g, v_g) are components of geostrophic wind velocity.

The Coriolis force is responsible for the wind veering with height, but there is no Coriolis force term in the default momentum equations for ANSYS Fluent 15.0. So, it is necessary to add the Coriolis force as source terms to the momentum equations by a user-defined function (UDF), which can be expressed as $S_x = \rho f v$ and $S_y = -\rho f u$ in the direction of x -axis and y -axis, respectively. Additionally, the Eq. (7) should also be embedded through the UDF source term to implement the modified k - ϵ model.

The computational results are obtained by setting the steady, 3d, double precision, pressure-based solver. The standard discretization scheme is applied to pressure, while second order upwind schemes are adopted for momentum and turbulence quantities, and the SIMPLEC algorithm is selected for pressure-velocity coupling. The convergence criteria of the scaled residuals for all variables and the continuity equation are set as 10^{-6} .

2.1.3 Results

Fig. 4 shows the precursor simulation results of wind profiles of mean velocity components, mean velocity magnitude, mean wind veering angle and non-dimensional turbulent kinetic energy (normalized by u_*^2 , only the selected values at the height range $z/h = 0\sim 3$ are exhibited to emphasize the results of k/u_*^2 at low altitude). To evaluate the reality of the simulated wind profiles, the field measurement data of ‘‘Leipzig Wind Profile’’ (Lettau 1950), Brost *et al.* (1982), and Grant (1986), the results derived from large eddy simulations (Esau 2004), classical Ekman model solution (Ekman 1905), the turbulent kinetic energy for ‘‘Leipzig Wind Profile’’ derived by Detering and Etling (1985), the profiles of mean velocity (also fitted by the logarithmic law with the values of $u_* = 0.577 \text{ m}\cdot\text{s}^{-1}$ and $z_0 = 2.25 \times 10^{-4} \text{ m}$ which are the same as the corresponding values for the scaled ‘‘Leipzig Wind Profile’’ in Table 1) and turbulent kinetic energy for the TJ-2 wind tunnel tests (Zheng *et al.* 2012) are also included in Fig. 4 for comparisons. In Fig. 4(e), the ABL height $h \approx 808 \text{ m}$ is taken to normalize the vertical coordinate z for the prototype of ‘‘Leipzig Wind Profile’’ as discussed in Subsection ‘‘Target wind profile’’ above.

As can be seen from Fig. 4, the modified k - ϵ model simulation results on three different mesh discretization schemes are close to each other and in good agreement with the field measurement data. The wind velocity and veering deviate slightly from the classical Ekman solution due to the constant eddy viscosity assumption for the Ekman model (the eddy viscosity $K = 0.0053 \text{ m}^2\cdot\text{s}^{-1}$ for the scaled model herein). It can also be observed that the field measurement data of turbulent kinetic energy are very scattered. Compared with the previous work, non-dimensional turbulent kinetic energy results of the precursor simulations are comparable to the corresponding results of Detering and Etling (1985) and are within the range of variation of the LES data (Esau 2004). The vertical variation in the simulated turbulent kinetic energy appears to be reasonable, and is an important feature that is currently being pursued in CFD modelling of the ABL turbulence (Yang *et al.* 2009).

Finally, it is worth noting that there are discrepancies between the mean wind profiles used in the conventional wind tunnel tests and the actual ABL. Specifically, the logarithmic law adopted for the mean wind velocity profile is valid only in the ASL, and its applicable height is approximately 100 m (Li *et al.* 2010, Drew *et al.* 2013). The logarithmic law used in the conventional wind tunnel tests underestimates the high-altitude wind speed and cannot reflect the features of inflection point or wind veering as the simulation results. Nevertheless, the turbulent kinetic energy profile used in the conventional wind tunnel tests is roughly reasonable, which can reflect the trend of the field-measured results of the ABL with height.

2.2 Main simulation

2.2.1 Simulations and implementations

Mesh discretization

The main simulations on different meshes are performed to check the requirement of mesh independence. The details about the three mesh discretization schemes are listed in Table 4. The size of the main simulation domain is $L \times B \times H = 9 \text{ m} \times 9 \text{ m} \times 3 \text{ m}$. The mesh size in horizontal and lateral direction is uniform and equals to 0.18 m, while the height of the first mesh layer above ground, Δ_m , and the vertical growing factor are set differently for the three meshes and are consistent with the corresponding values in the precursor simulations mentioned above. The mesh discretization scheme named ‘‘Self-sustain-b’’ in Table 4 is assigned as the basic mesh model hereinafter.

Boundary conditions and solving settings

The analysis above shows that a realistic ABL flow results from a balance of the horizontal pressure gradient force, the Coriolis force, and the turbulent stress divergence. However, in wind engineering applications, the flow relies only on the driving of the inlet boundary if the whole depth of the ABL is simulated (Cai *et al.* 2014). Applying the wind profiles derived by the precursor simulations as inflow conditions, the main simulations are undertaken to determine whether or not the ‘‘boundary-driven’’ flow remains horizontally homogeneous. Profiles of wind velocity, turbulent kinetic energy, and its dissipation rate are used to ‘‘drive’’ the ABL flow in the respective empty simulation domains.

Besides, it is worth mentioning that as can be seen from Fig. 4, the mean wind velocity magnitude exceeds the geostrophic wind velocity G in a certain height range, and after the mean wind direction is parallel to the geostrophic wind direction for the first time, the wind velocity component v perpendicular to the geostrophic wind G will have a negative value with the increase of height, which has been confirmed by many field measurements and theoretical analyses (Zhao 2006). This common feature of the conventionally neutral ABL — the development of a super-geostrophic jet near the top of the boundary layer — complicates the lateral boundary condition, and the reverse flow at the lateral boundaries should become a general case, meaning that the inflow and outflow boundaries cannot be clearly defined (Cai *et al.* 2014). In order to overcome this difficulty, the overall inflow can be rotated by a certain

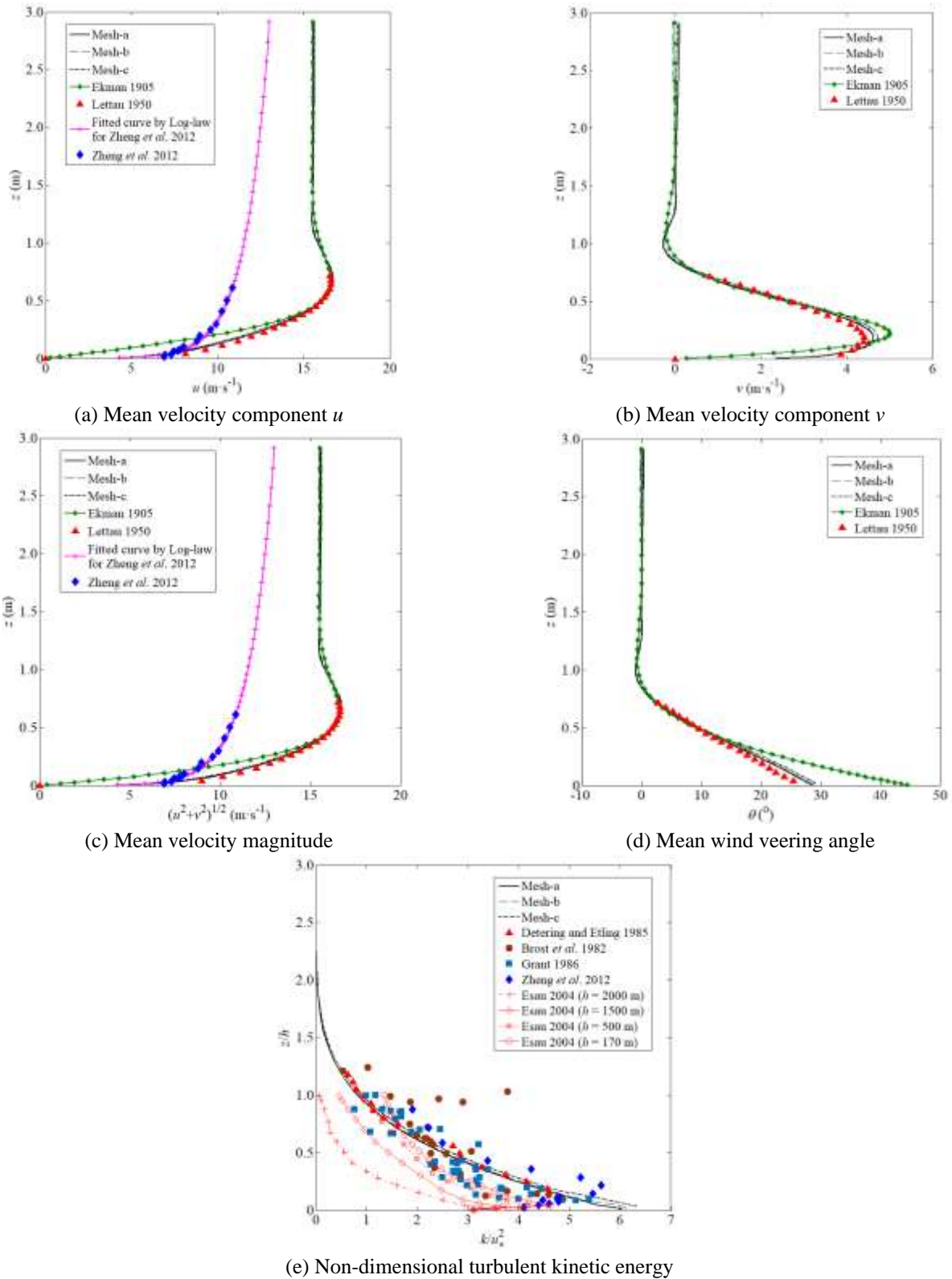


Fig. 4 The ABL precursor simulation results and comparisons

degree while the outline of the fluid domain remains unchanged. For convenience, the inflow will be rotated clockwise by 26.1° (i.e., the angle between the surface wind and the geostrophic wind, see Table 1). That is, the “Original Surface Wind” (OSW) and the “Original Geostrophic Wind” (OGW) will be rotated to the locations

of the “New Surface Wind” (NSW) and “New Geostrophic Wind” (NGW) respectively, as shown in Fig. 5 below. The new inflow condition is relatively reasonable, and there will be no reverse flow at the outflow boundary.

The boundary conditions for main simulations are shown in Fig. 6. Overall, the main simulations correspond

Table 4 Mesh discretization schemes for main simulations

Cases	Number of cells ($N_x \times N_y \times N_z$)*	Height of the first mesh layer above ground d_m (m)	Vertical growing factor	Dimensionless wall unit y^+
Self-sustain-a	50×50×50	0.01	1.06	265~292
Self-sustain-b	50×50×50	0.02	1.04	450~498
Self-sustain-c	50×50×30	0.04	1.06	820~923

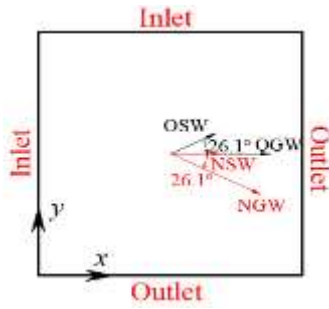


Fig. 5 Overall inflow rotation diagram

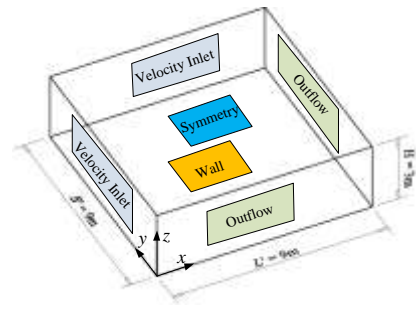


Fig. 6 Boundary conditions for main simulations

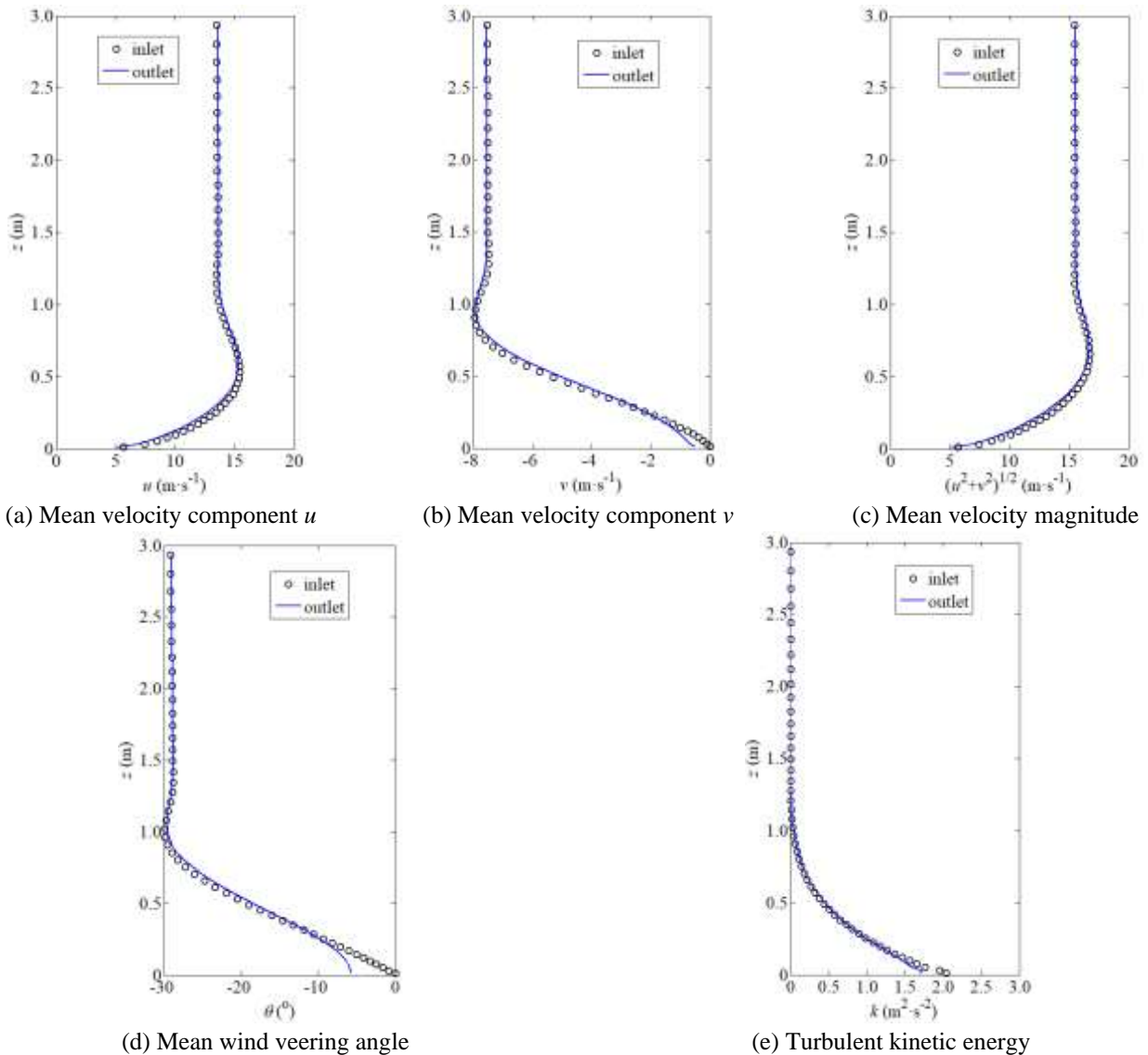


Fig. 7 Comparisons of profiles at the inlet and outlet for the basic mesh model in the main simulation

to the precursor simulations, and have the same settings as described in Subsection 2.1.2 except that: (a) simulation domains with longer horizontal and lateral scales (9 m) are taken; (b) the horizontal and lateral grid size is $\Delta_x = \Delta_y = 0.18$ m; (c) inlet conditions are adopted from the resulting profiles of the corresponding precursor simulations; (d) outlet takes the outflow condition; (e) no source term (the Coriolis force) is used in the momentum equations; and (f) the horizontal pressure gradient is not applied.

2.2.2 Results

Numerical results of the basic mesh model

Fig. 7 depicts the comparison results between the inlet and outlet for the basic mesh model (i.e., “Self-sustain-b”) in the main simulation, including the profiles of mean velocity components, mean velocity magnitude, mean wind veering angle and turbulent kinetic energy. It can be observed that the profiles of these physical quantities are sustained well throughout the domain under the present model settings, except for small regions near the ground.

The main reason for this error is that only a small number of grids are used for the precursor simulations of the ABL, i.e., the precursor simulation domain is only equivalent to the “sub-domain” of the main simulation. On the other hand, the horizontal pressure gradient is responsible for the horizontal motion of air and the Coriolis force contributes to the wind veering with height in the precursor simulations, while the flow relies only on the driving of the inlet boundary and the wind veering is also introduced from the inlet boundary in the main simulations. Therefore, the decay or deformation of the “boundary-driven” ABL flow in the downstream region for the main simulations is unavoidable.

Verification of mesh independence

As mentioned above, the main simulations on three different meshes (shown in Table 4) are performed to verify the requirement of mesh independence. Fig. 8 illustrates the corresponding simulation results of these mesh schemes at the outlet, in which only the values at the height range 0~1.6 m are exhibited to underline the results at low altitude.

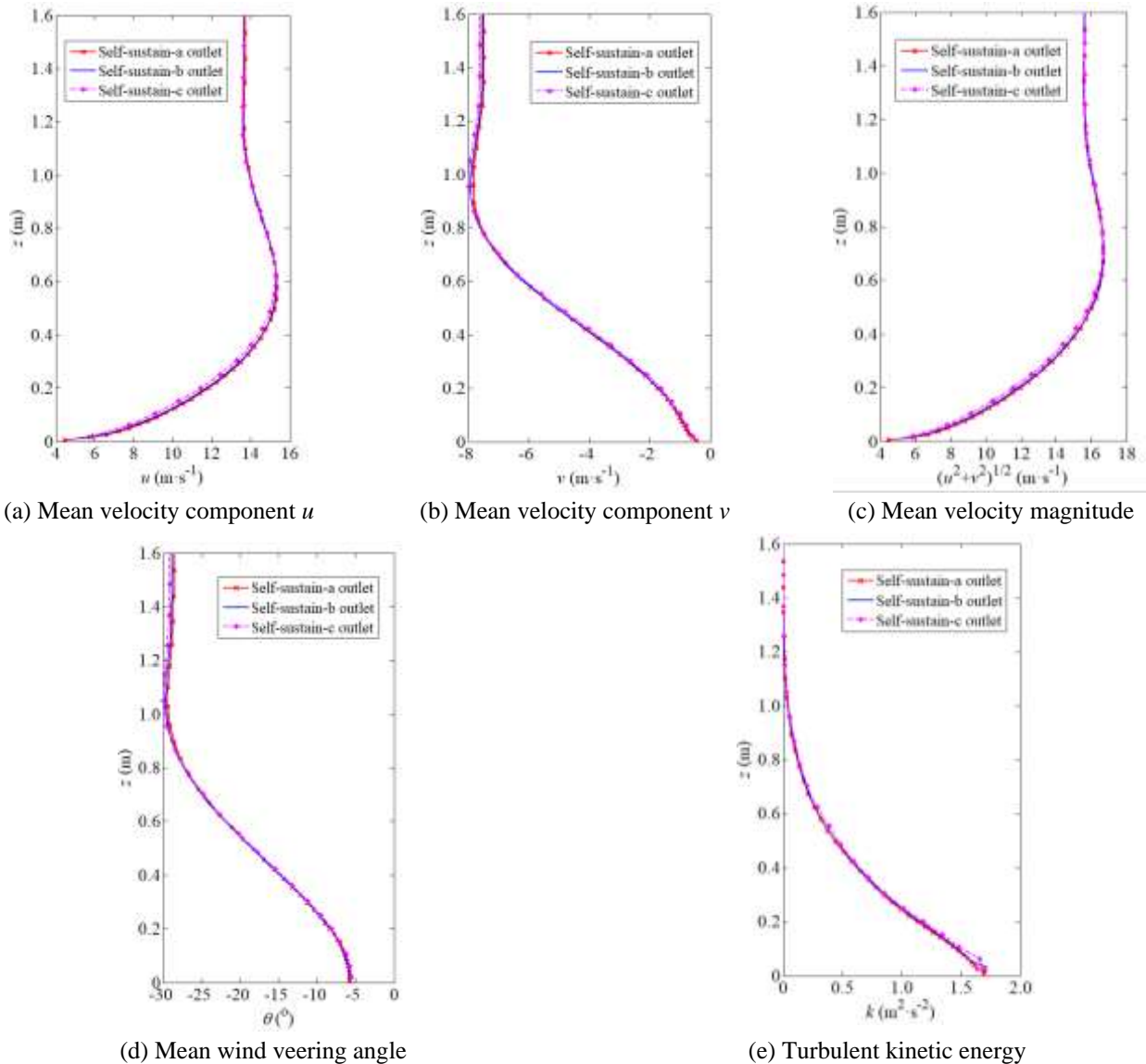


Fig. 8 Comparisons of profiles at the outlet among the three mesh schemes in the main simulations

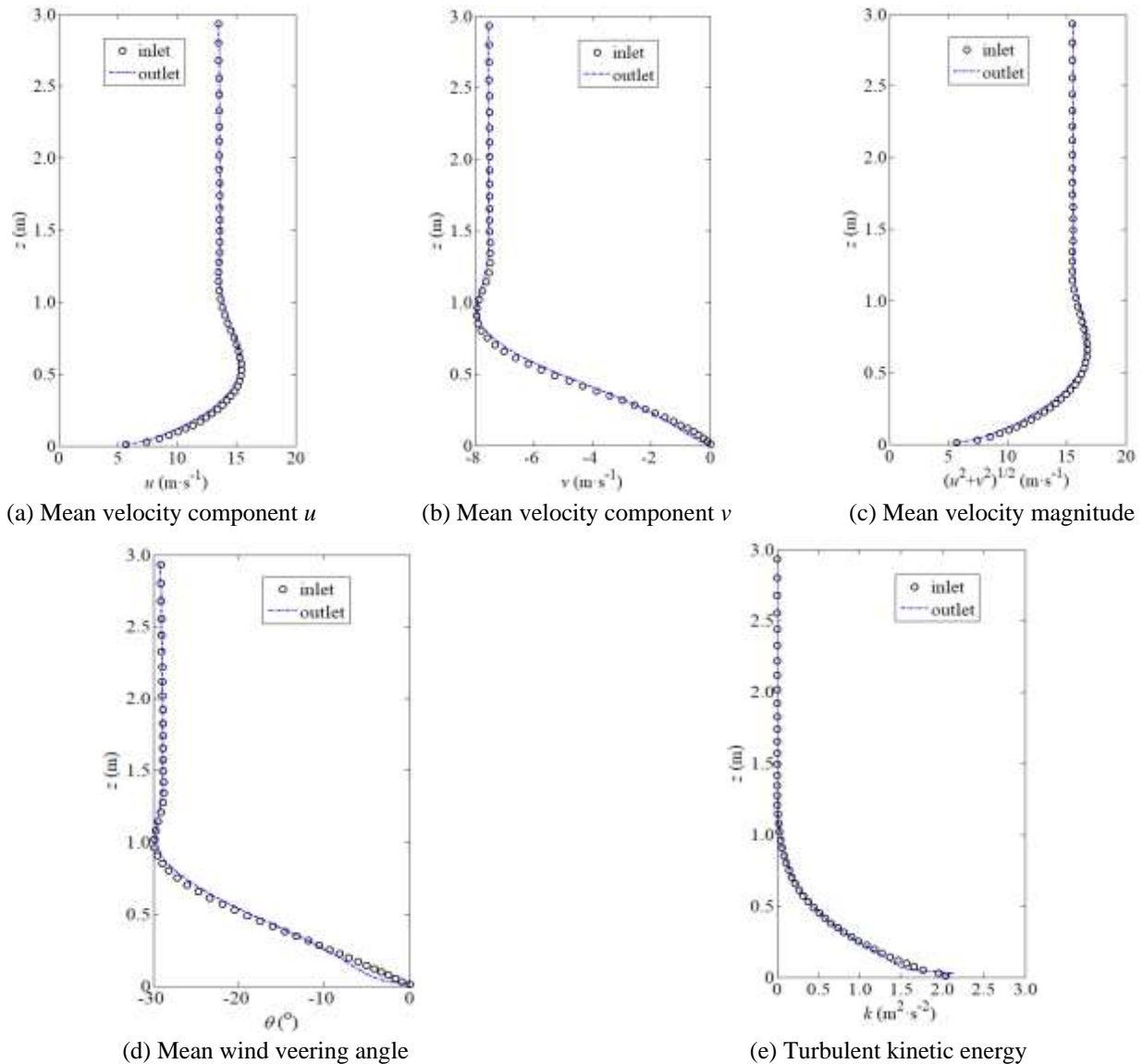


Fig. 9 Comparisons of profiles at the inlet and outlet for the basic mesh model with near-ground adjustment

It can be seen that the simulated profiles at the outlet on different meshes are very close to each other. When considered in conjunction with the comparison results between the inlet and outlet shown in Fig. 7, it can be concluded that all the physical quantities of the three mesh schemes are self-sustained well despite some deviations near ground, and the numerical simulation method proposed in this section is independent of the mesh discretization schemes.

2.3 Near-ground physical quantities adjustment

2.3.1 Near-ground physical quantities adjustment measures

In view of the fact that the error mainly occurs near ground, the near-ground physical quantities can be adjusted slightly in order to achieve better self-sustaining results. It is proposed to use the method of specifying the fixed velocity, turbulent kinetic energy and turbulent energy dissipation rate to the one cell thick “sub-domain” nearest

the ground in this section, which is called “near-ground physical quantities adjustment” or “near-ground adjustment” hereinafter.

In ANSYS Fluent 15.0, Fixed Values option can be enabled if you want to fix the values of one or more variables in the fluid zone, rather than computing them during the calculation. This option essentially allows you to set a boundary condition for the variables within the cells of the zone, and the physical quantities in the rest of the domain can then be calculated using these fixed values as a boundary condition. More specifically, first, a one cell thick “sub-domain” at the ground boundary should be created during meshing, and then, the Fixed Values option should be enabled in the Fluid Dialog Box and the near-ground physical quantities which coincide with the values of inflow profiles at the corresponding location should be specified to the one cell thick “sub-domain”, and finally, the original wall boundary condition at ground should be changed to the symmetry boundary.

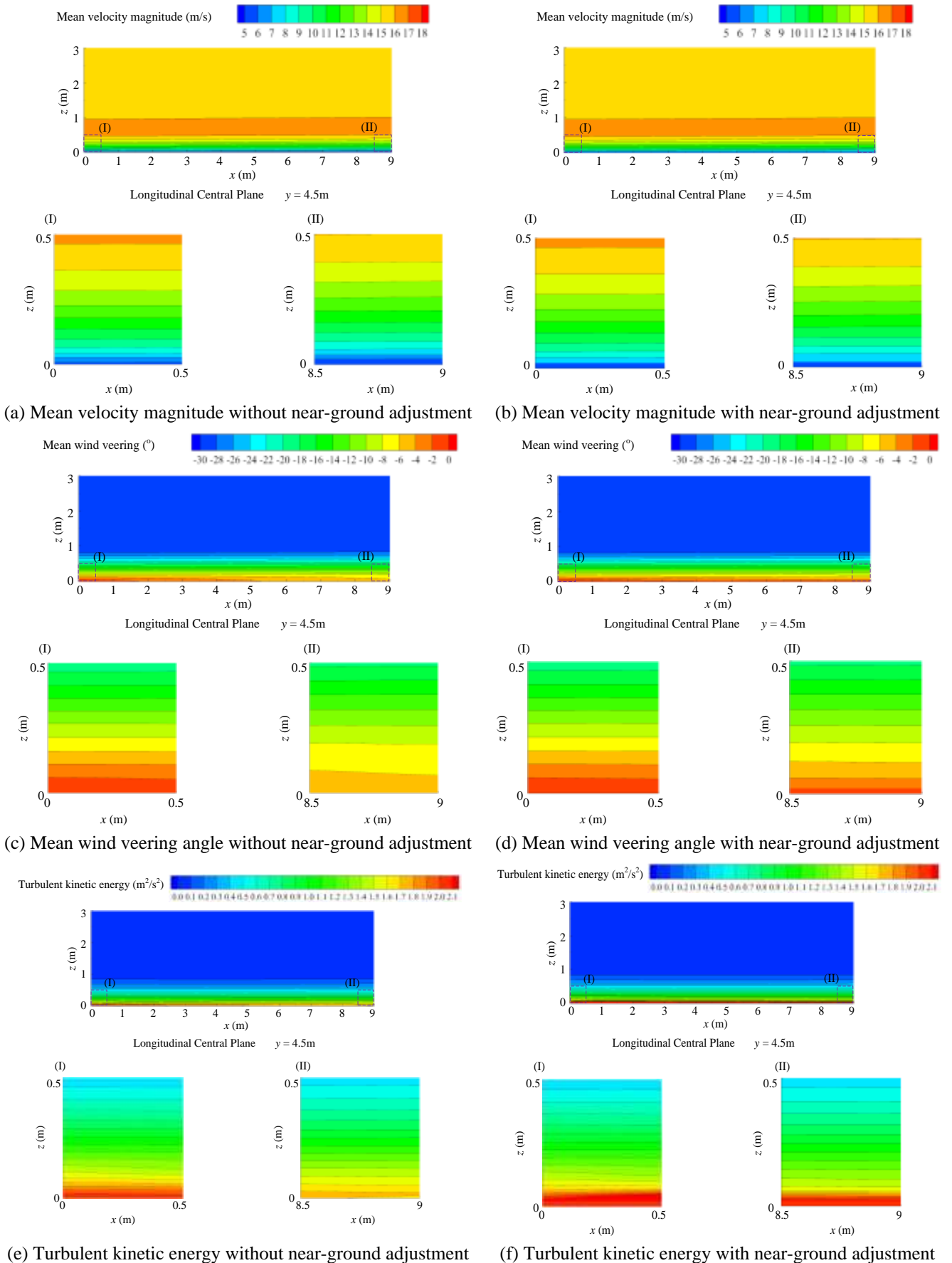


Fig. 10 Contours of mean velocity magnitude, mean wind veering and turbulent kinetic energy on the longitudinal central plane ($y = 4.5\text{ m}$) with and without near-ground adjustment for the basic mesh model

2.3.2 Results

Numerical results of the basic mesh model

Fig. 9 depicts the comparison results between the inlet and outlet for the basic mesh model (i.e., “Self-sustain-b”) with the near-ground adjustment. When compared with the results in Fig. 7, it can be found that the profiles of all physical quantities are sustained more satisfactorily throughout the domain with the near-ground adjustment.

To be more intuitive, the contours of mean velocity magnitude, mean wind veering and turbulent kinetic energy on the longitudinal central plane ($y = 4.5$ m) with and without near-ground adjustment for the basic mesh model are shown in Fig. 10. In order to display the discrepancies between the inlet and outlet more clearly, the close-up views of the near-inlet and low-altitude region (marked by “(I)”), and of the near-outlet and low-altitude region (marked by “(II)”) are exhibited in Figs. 10(a)-10(f). It can be observed that through specifying the consistent flow quantities to the near-ground cell, the favorable effects are not only confined to the one cell thick region as such, but also extended to higher altitudes above ground ($z = 0\sim 0.5$ m). This phenomenon further highlights the accuracy and effectiveness of the adjustment measures adopted in this section.

Relative errors between the inlet and outlet

In this subsection, the relative errors of mean velocity magnitude, mean wind veering angle and turbulent kinetic energy between the inlet and outlet are analysed quantitatively, which are defined as Eqs. (16)-(18), respectively

$$error_mag(\%) = 100 \frac{U_{outlet} - U_{inlet}}{U_{inlet}} \quad (16)$$

$$error_theta(\%) = 100 \frac{\theta_{outlet} - \theta_{inlet}}{\theta_0} \quad (17)$$

$$error_k(\%) = 100 \frac{k_{outlet} - k_{inlet}}{k_0} \quad (18)$$

where the subscripts “inlet” and “outlet” denote the physical quantities at the inlet and outlet, respectively; U , θ and k represent the mean wind velocity magnitude, mean wind veering angle and turbulent kinetic energy, respectively; θ_0 is the total wind veering angle between the surface wind and the geostrophic wind ($\theta_0 = 26.1^\circ$, see Table 1); and k_0 is defined as $k_0 = u_*^2 / C_\mu^{1/2}$. In view of near-zero values for the mean wind veering near ground and turbulent kinetic energy at high altitude, the denominators on the right-hand side of Eqs. (17) and (18) are designated as constants.

Figs. 11-13 illustrate the relative errors of mean velocity magnitude, mean wind veering angle and turbulent kinetic energy between the inlet and outlet for the three different meshes, respectively. As shown in figures, the maximum relative error of the mean velocity magnitude does not exceed 7% with the near-ground adjustment, while the maximum relative error ranges from 8% to 12% without the near-ground adjustment. The near-ground adjustment measures also contribute to more satisfactory horizontal homogeneity of the mean wind veering angle and turbulent kinetic energy, and their maximum relative errors decrease to just 1/3~1/2 of the corresponding errors in the cases without the near-ground adjustment. Meanwhile, the distribution patterns of the relative errors with height for different mesh discretization schemes are very similar, indicating that the effectiveness of the near-ground physical quantities adjustment measures is independent of the adopted meshes.

3. Conclusions

In this paper, a modified $k-\varepsilon$ model has been introduced for the ABL simulation considering wind veering. The self sustainable method including the precursor simulation,

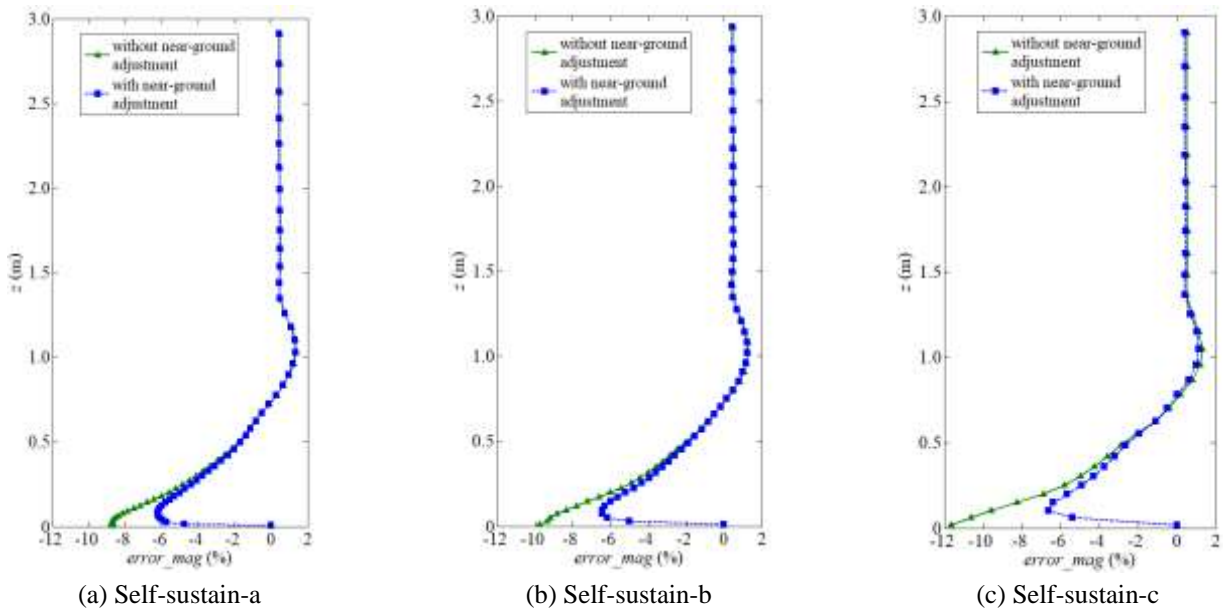


Fig. 11 Relative errors of mean velocity magnitude between the inlet and outlet for three different meshes

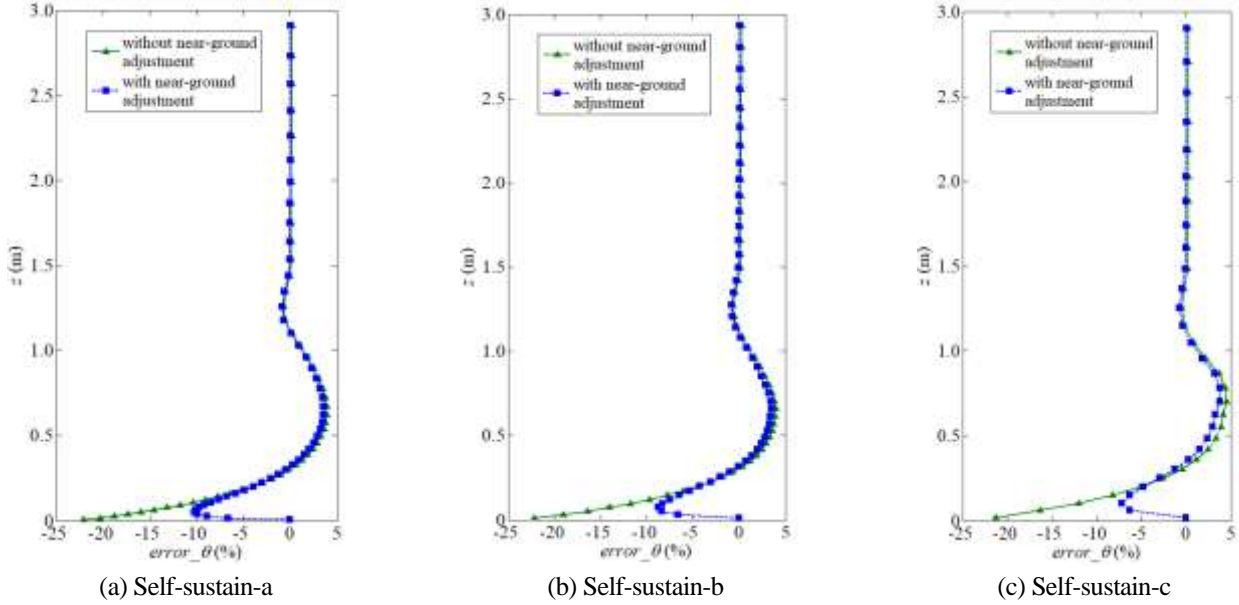


Fig. 12 Relative errors of mean wind veering angle between the inlet and outlet for three different meshes

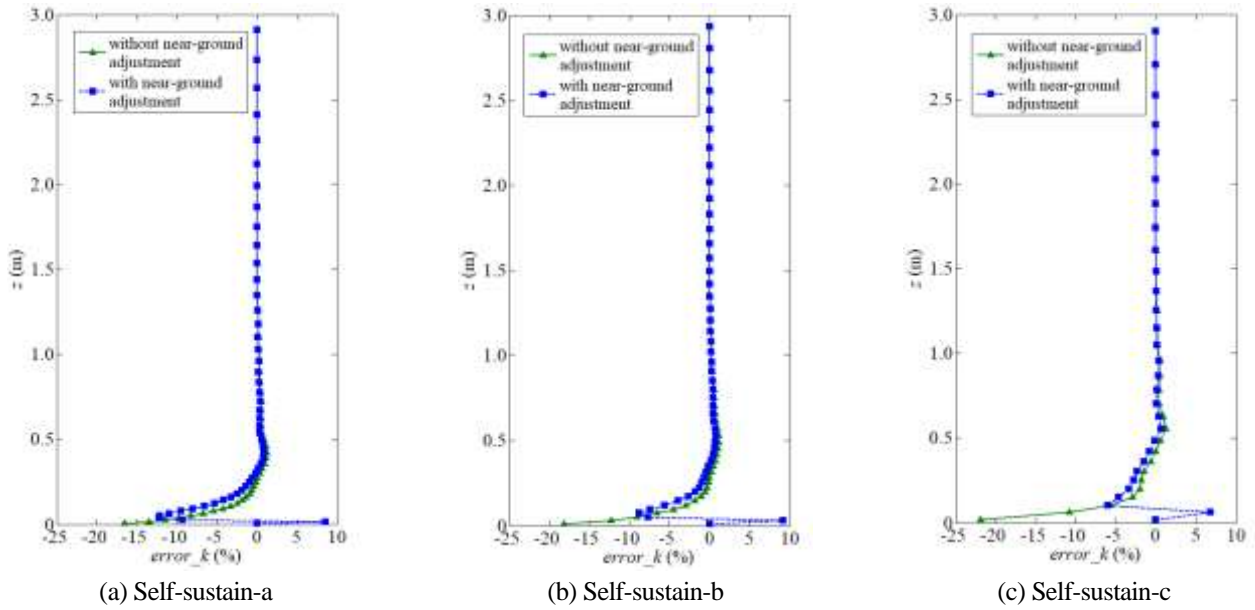


Fig. 13 Relative errors of turbulent kinetic energy between the inlet and outlet for three different meshes

main simulation and near-ground physical quantities adjustment has been discussed in detail, and the capability of this method has been numerically verified. The main conclusions of this paper can be summarized as follows:

- Through the modification to the standard $k-\varepsilon$ model, namely, by modifying the parameter $C_{1\varepsilon}$ in the ε equation to establish a feedback mechanism that prevents the turbulent length scale from exceeding the maximum mixing length of the ABL, more consistent simulation results with the field measurement data can be obtained.
- When applying the wind profiles derived by the precursor simulations as inflow conditions in the main simulations, the mean wind velocity, mean wind veering and turbulent kinetic energy can all be self-sustained well in empty domains.
- The near-ground physical quantities adjustment measures will contribute to more satisfactory self-sustainable results by means of specifying the consistent flow quantities to the near-ground cell.
- It should be noted that the logarithmic law adopted for the mean wind velocity profile is valid only in the ASL, and its applicable height is approximately 100m. The logarithmic law used in the conventional wind tunnel tests underestimates the high-altitude wind speed and cannot reflect the features of inflection point or wind veering, so it is not appropriate for the design of thousand-meter super high-rise buildings.

The aim of this paper is to explore a relatively precise and concise way to define the inflow boundary conditions for numerical simulations considering wind veering effects, and to seek an efficient method to simulate the corresponding self-sustainable ABL. Although this study has built on the modification to the standard $k-\varepsilon$ model, the self-sustainable method would be potentially valuable of being extended to other RANS models, such as Realizable $k-\varepsilon$ model, SST $k-\omega$ model, etc. Furthermore, the simulated profiles of mean wind velocity, mean wind veering, turbulent kinetic energy and its dissipation rate can be utilized for the inflow turbulence generation in large eddy simulation (LES) of wind loads on super high-rise buildings subsequently. Nevertheless, more efforts still need to be done to clarify the consequences of the modification to the turbulence model itself when applied to the building flow simulations, and to verify the accuracy and effectiveness of the ABL flow simulation method considering wind veering in the numerical wind-resistance design of thousand-meter super high-rise buildings.

Acknowledgments

The authors gratefully acknowledge the support from the National Natural Science Foundation of China (90715040, 91215302) and State Key Laboratory for Disaster Reduction in Civil Engineering (SLDRCE15-A-04, SLDRCE19-A-05). The authors would like to express special gratitude to Dr. Zheng Chaorong from Harbin Institute of Technology for helpful discussions.

References

- Andren, A., Brown, A.R., Graf, J., Mason, P.J., Moeng, C.H., Nieuwstadt, F.T.M. and Schumann, U. (1994), "Large-eddy simulation of a neutrally stratified boundary layer: A comparison of four computer codes", *Q. J. R. Meteorol. Soc.*, **120**(520), 1457-1484. <https://doi.org/10.1002/qj.49712052003>.
- Apsley, D.D. and Castro, I.P. (1997), "A limited-length-scale $k-\varepsilon$ model for the neutral and stably-stratified atmospheric boundary layer", *Bound.-Lay. Meteorol.*, **83**(1), 75-98. <https://doi.org/10.1023/A:1000252210512>.
- Blackadar, A.K. (1962), "The vertical distribution of wind and turbulent exchange in a neutral atmosphere", *J. Geophys. Res.*, **67**(8), 3095-3102. <https://doi.org/10.1029/JZ067i008p03095>.
- Blocken, B., Stathopoulos, T. and Carmeliet, J. (2007), "CFD simulation of the atmospheric boundary layer: wall function problems", *Atmos. Environ.*, **41**(2), 238-252. <https://doi.org/10.1016/j.atmosenv.2006.08.019>.
- Brost, R.A., Wyngaard, J.C. and Lenschow, D.H. (1982), "Marine stratocumulus layers. Part II: Turbulence budgets", *J. Atmos. Sci.*, **39**(4), 818-836. [https://doi.org/10.1175/15200469\(1982\)039<0818:MSLPIT>2.0.CO;2](https://doi.org/10.1175/15200469(1982)039<0818:MSLPIT>2.0.CO;2).
- Cai, X.H., Huo, Q., Kang, L. and Song, Y. (2014), "Equilibrium atmospheric boundary-layer flow: computational fluid dynamics simulation with balanced forces", *Bound.-Lay. Meteorol.*, **152**(3), 349-366. <https://doi.org/10.1007/s10546-014-9928-0>.
- Detering, H.W. and Etling, D. (1985), "Application of the $E-\varepsilon$ turbulence model to the atmospheric boundary layer", *Bound.-Lay. Meteorol.*, **33**(2), 113-133. <https://doi.org/10.1007/BF00123386>.
- Drew, D.R., Barlow, J.F. and Lane, S.E. (2013), "Observations of wind speed profiles over Greater London, UK, using a Doppler lidar", *J. Wind Eng. Ind. Aerod.*, **121**, 98-105. <https://doi.org/10.1016/j.jweia.2013.07.019>.
- Duynkerke, P.G. (1988), "Application of the $E-\varepsilon$ turbulence closure model to the neutral and stable atmospheric boundary layer", *J. Atmos. Sci.*, **45**(5), 865-880. [https://doi.org/10.1175/15200469\(1988\)045<0865:AOTTCM>2.0.CO;2](https://doi.org/10.1175/15200469(1988)045<0865:AOTTCM>2.0.CO;2).
- Ekman, V.W. (1905), "On the influence of the earth's rotation on ocean-currents", *Ark. Mat. Astr. Fys.*, **2**, 1-52.
- Esau, I. (2004), "Simulation of Ekman boundary layers by large eddy model with dynamic mixed subfilter closure", *Environ. Fluid Mech.*, **4**(3), 273-303. <https://doi.org/10.1023/B:EFMC.0000024236.38450.8d>.
- Franke, J., Hellsten, A., Schlünzen, H. and Carissimo, B. (2007), *Best Practice Guideline for the CFD Simulation of Flows in the Urban Environment*, COST Office, Brussels, Belgium.
- Grant, A.L.M. (1986), "Observations of boundary layer structure made during the 1981 KONTUR experiment", *Q. J. R. Meteorol. Soc.*, **112**(473), 825-841. <https://doi.org/10.1002/qj.49711247314>.
- He, Y.C., Chan, P.W. and Li, Q.S. (2013), "Wind profiles of tropical cyclones as observed by Doppler wind profiler and anemometer", *Wind Struct., Int. J.*, **17**(4), 419-433. <https://doi.org/10.12989/was.2013.17.4.419>.
- Koblitz, T., Bechmann, A., Sogachev, A., Sørensen, N. and Réthoré, P.E. (2015), "Computational Fluid Dynamics model of stratified atmospheric boundary-layer flow", *Wind Energy*, **18**(1), 75-89. <https://doi.org/10.1002/we.1684>.
- Launder, B.E. and Spalding, D.B. (1974), "The numerical computation of turbulent flows", *Comput. Method. Appl. M.*, **3**(2), 269-289. [https://doi.org/10.1016/0045-7825\(74\)90029-2](https://doi.org/10.1016/0045-7825(74)90029-2).
- Lettau, H. (1950), "A re-examination of the "Leipzig wind profile" considering some relations between wind and turbulence in the frictional layer", *Tellus*, **2**(2), 125-129. <https://doi.org/10.3402/tellusa.v2i2.8534>.
- Li, B., Yang, Q., Solari, G. and Wu, D. (2017), "Investigation of wind load on 1,000 m high super-tall buildings based on HFFB tests", *Struct. Control. Health.*, **25**, e2068. <https://doi.org/10.1002/stc.2068>.
- Li, Q.S., Zhi, L. and Hu, F. (2010), "Boundary layer wind structure from observations on a 325 m tower", *J. Wind Eng. Ind. Aerod.*, **98**(12), 818-832. <https://doi.org/10.1016/j.jweia.2010.08.001>.
- Liu, Z., Zheng, C., Wu, Y. and Song, Y. (2018), "Investigation on characteristics of thousand-meter height wind profiles at non-tropical cyclone prone areas based on field measurement", *Build. Environ.*, **130**, 62-73. <https://doi.org/10.1016/j.buildenv.2017.12.001>.
- O'Sullivan, J.P., Archer, R.A. and Flay, R.G.J. (2011), "Consistent boundary conditions for flows within the atmospheric boundary layer", *J. Wind Eng. Ind. Aerod.*, **99**(1), 65-77. <https://doi.org/10.1016/j.jweia.2010.10.009>.
- Pedersen, J.G., Gryning, S.E. and Kelly, M. (2014), "On the structure and adjustment of inversion-capped neutral atmospheric boundary-layer flows: Large-eddy simulation study", *Bound.-Lay. Meteorol.*, **153**(1), 43-62. <https://doi.org/10.1007/s10546-014-9937-z>.
- Peña, A., Gryning, S.E. and Floors, R. (2014), "The turning of the wind in the atmospheric boundary layer", *J. Phys.: Conf. Ser.*, **524**(1), 012118. <https://doi.org/10.1088/1742-6596/524/1/012118>.
- Poroseva, S. and Iaccarino, G. (2001), "Simulating separated flow using $k-\varepsilon$ model", Annual Research Briefs 2001; Centre for Turbulence Research, Stanford University.
- Richards, P.J. and Hoxey, R.P. (1993), "Appropriate boundary

- conditions for computational wind engineering models using the k - ϵ turbulence model”, *J. Wind Eng. Ind. Aerod.*, **46-47**, 145-153. [https://doi.org/10.1016/0167-6105\(93\)90124-7](https://doi.org/10.1016/0167-6105(93)90124-7).
- Riopelle, G. and Stubble, G.D. (1989), “The influence of atmospheric stability on the ‘Leipzig’ boundary-layer structure”, *Bound.-Lay. Meteorol.*, **46(3)**, 207-227. <https://doi.org/10.1007/BF00120840>.
- Simiu, E. and Scanlan, R.H. (1996), *Wind Effects on Structures: Fundamentals and Applications to Design*, John Wiley & Sons, New York, NY, USA.
- Sogachev, A., Kelly, M. and Leclerc, M.Y. (2012), “Consistent two-equation closure modelling for atmospheric research: buoyancy and vegetation implementations”, *Bound.-Lay. Meteorol.*, **145(2)**, 307-327. <https://doi.org/10.1007/s10546-012-9726-5>.
- Tamura, Y., Suda, K., Sasaki, A., Iwatani, Y., Fujii, K., Ishibashi, R. and Hibi, K. (2001), “Simultaneous measurements of wind speed profiles at two sites using Doppler sodars”, *J. Wind Eng. Ind. Aerod.*, **89(3-4)**, 325-335. [https://doi.org/10.1016/S0167-6105\(00\)00085-4](https://doi.org/10.1016/S0167-6105(00)00085-4).
- Tamura, Y., Iwatani, Y., Hibi, K., Suda, K., Nakamura, O., Maruyama, T. and Ishibashi, R. (2007), “Profiles of mean wind speeds and vertical turbulence intensities measured at seashore and two inland sites using Doppler sodars”, *J. Wind Eng. Ind. Aerod.*, **95(6)**, 411-427. <https://doi.org/10.1016/j.jweia.2006.08.005>.
- Tse, K.T., Weerasuriya, A.U. and Kwok, K.C.S. (2016), “Simulation of twisted wind flows in a boundary layer wind tunnel for pedestrian-level wind tunnel tests”, *J. Wind Eng. Ind. Aerod.*, **159**, 99-109. <https://doi.org/10.1016/j.jweia.2016.10.010>.
- Weerasuriya, A.U., Hu, Z., Zhang, X., Tse, K.T., Li, S. and Chan, P.W. (2018), “New inflow boundary conditions for modeling twisted wind profiles in CFD simulation for evaluating the pedestrian-level wind field near an isolated building”, *Build. Environ.*, **132**, 303-318. <https://doi.org/10.1016/j.buildenv.2018.01.047>.
- Yang, W., Quan, Y., Jin, X.Y., Tamura, Y. and Gu, M. (2008), “Influences of equilibrium atmosphere boundary layer and turbulence parameter on wind loads of low-rise buildings”, *J. Wind Eng. Ind. Aerod.*, **96(10-11)**, 2080-2092. <https://doi.org/10.1016/j.jweia.2008.02.014>.
- Yang, Y., Gu, M., Chen, S.Q. and Jin, X.Y. (2009), “New inflow boundary conditions for modelling the neutral equilibrium atmospheric boundary layer in computational wind engineering”, *J. Wind Eng. Ind. Aerod.*, **97(2)**, 88-95. <https://doi.org/10.1016/j.jweia.2008.12.001>.
- Yang, Y., Xie, Z. and Gu, M. (2017), “Consistent inflow boundary conditions for modelling the neutral equilibrium atmospheric boundary layer for the SST k - ω model”, *Wind Struct., Int. J.*, **24(5)**, 465-480. <https://doi.org/10.12989/was.2017.24.5.465>.
- Yeo, D. (2012), “Practical estimation of veering effects on high-rise structures: a database-assisted design approach”, *Wind Struct., Int. J.*, **15(5)**, 355-367. <https://doi.org/10.12989/was.2012.15.5.355>.
- Zhao, M. (2006), *Atmospheric Boundary Layer Dynamics*, Higher Education Press, Beijing, China.
- Zheng, D.Q., Zhang, A.S. and Gu, M. (2012), “Improvement of inflow boundary condition in large eddy simulation of flow around tall building”, *Eng. Appl. Comp. Fluid*, **6(4)**, 633-647. <https://doi.org/10.1080/19942060.2012.11015448>.
- Zilitinkevich, S.S. and Esau, I.N. (2002), “On integral measures of the neutral barotropic planetary boundary layer”, *Bound.-Lay. Meteorol.*, **104(3)**, 371-379. <https://doi.org/10.1023/A:1016540808958>.
- Zilitinkevich, S., Esau, I. and Baklanov, A. (2007), “Further comments on the equilibrium height of neutral and stable planetary boundary layers”, *Q.J.R. Meteorol. Soc.*, **133(622)**, 265-271. <https://doi.org/10.1002/qj.27>.

FR